Journal of Sound and Vibration (2002) **251**(5), 807–822
doi:10.1006/jsvi.2001.3998, available online at http://www.idealibrary.com on IDEAL®

DYNAMIC BEHAVIOR OF THE FULL ROTOR/STOP RUBBING: NUMERICAL SIMULATION AND EXPERIMENTAL VERIFICATION

X. Dai, Z. Jin and X. Zhang

Department of Engineering Physics, Tsinghua University, Beijing 100084, *People's Republic of China.*
E-mails: daixj@dns.ep.tsinghua.edu.cn, daixingjian@263.net

(*Received* 9 *January* 2001, *and in final form* 10 *August* 2001)

The dynamic behavior of a rotor rubbing, especially rubbing fully with a motion-limiting stop is investigated by numerical and experimental methods. In the dynamic simulation, the sinuous excitation force with low frequency excites the large whirl of the unbalanced rotor and thus causes the rubbing between the rotor and the stop. The simple Coulomb friction model and the multiple segments linear spring model are used to reveal the nature of the rubbing forces. The torque equation of the rotor is built to extract the rotating speed during partial and full rubbing. The stable partial rubbing motion demonstrates that the stop limits the violent vibration amplitude of the rotor effectively. The rubbing experiments confirm the idea of using the inner type of stop to suppress the violent backward whirl with low frequency. When the amplitude of the excitation force exceeds a certain value, the full rubbing occurs with serious continuous friction. During full rubbing, the center of the rotor moves counter-clockwise and whips in the amplitude exceeding the rotor/stop gap dramatically. Moreover, the whip frequency is much higher than the frequencies of the excitation and the unbalance force. And then the rotor rotation is broken quickly by the stop. The predicted dynamical behavior is verified by the rubbing experiments. The relation between the stop/bearing stiffness ratio and such dynamical behavior as the initiation of the rubbing, the over-limit ratio and the contact-ratio is discussed.

1. INTRODUCTION

The motion-limiting stop is designed to restrict the violent vibration of mechanical systems such as beams or rotor-bearing systems. The stop works under impacts and rubs if the vibration amplitude exceeds the gap between the rotor and the stop. The clearance, impact and rub in mechanical vibration systems introduce non-linearity and complexity into the dynamic behavior. Much research has been carried out to understand the motion with rubbing and to find ways to prevent serious damages resulting from the unstable rubbing vibration.

Childs studied the stability of rotor/casing systems with rubbing and provided designers with valuable information on the performance of rotor systems under steady state–light rub interaction [1]. Matsushita focused on the vibration features of the rotor contacting with a stop in a fine gap used to suppress the rotor's seismic response [2]. Choy's non-linear analytical rotor–casing rub interaction simulation yielded insight into the interrelationship between rub force histories, energy levels, rub duration, incidence separation angles, and backward whirl initiation, as well as the overall rotor orbit during successive rubs [3]. The numerical simulation results presented by Goldman exhibited the orderly and chaotic behavior of rotors with rubs [4, 5]. Erich [6, 7], Chu and Zhang [8] discussed the

0022-460X/02/$35.00

non-linear phenomena in the dynamic response of rotors with rub impacts. Dai and Zhang [9] calculated the forced response of a precession rotor having impacts and rubs with a stop by the numerical integration method. Yanabe *et al.* [10] investigated the rotor vibration due to collision with an annular guard during passage through its critical speed. His analytical results confirmed that the rotor executed a diverging backward whirl due to the friction force during the collision and cannot pass through the critical speed in some cases. Isshi and Kirk [11], Flowers *et al.* [12] and Wang and Noah [13] investigated the auxiliary bearing as a critical feature of any magnetic bearing system in which rotor to auxiliary bearing rubs will probably occur.

Compared with theoretical analysis, the experimental results of the dynamic behavior of rotor-bearing systems with rubs are fewer because the rubbing experiments are difficult to carry out as well as dangerous. Muszynska *et al.* [14] designed rotor/stator rub experimental rig to study the partial rubbing at several locations and their effects on rotor dynamic responses. Free and Flowers [15] provided the experimental data of rotor-magnetic-bearing systems vibration when the rotor drops onto the auxiliary (back up) bearing.

The dynamic behavior of the rotor with rubbing especially with full rubbing is still unclear. The results of experiments on full rubbing are absent in publications. This paper is presented to investigate the motion of the rotor with full rubbing by numerical simulation and experimental methods. Contrary to the other dynamic models of rubbing rotors, the rotor is excited both by the unbalance force and by the low-frequency external excitation that causes the violent asynchronous backward whirl of the rotor. At the same time, the torque equation of the rotor is built to extract the rotating speed during partial and full rubbing. Experimental results about the rotor/stop rubbing are also provided. The predicted characters of the rotor under partial and full rubbing are confirmed well by the test data from experiments.

2. ROTOR-BEARING-STOP SYSTEM'S DYNAMIC MODEL

The support of the rotor is very flexible in some rotating machinery such as flywheels for energy storage, washing machines and centrifuges. Flexibility and difficulty in designing damping induce the rotor to whirl in its natural mode with low frequency under abnormal conditions such as earthquake events and other violent disturbances. Therefore, the motion-limiting stop is utilized to restrict the violent whirl of the rotor. As shown in Figure 1, a cylindrical rotor is presented to study the vibration of the rotor with partial and full rubbing. The stop is designed inside the hollow rotor top with a proper clearance (illustrated by Figure 1) to suppress the whirl of the rotor when the whirl amplitude of the rotor shaft center exceeds the rotor/stop gap. Collision and friction between the stop and the inner face of the rotor running at high speed occurs when the stop acts. The rotor/stop rubbing at the designed position prevents the rotor from rubbing with stationary parts at other positions. The stop does not work under normal conditions since the gap is much greater than the normal vibration amplitude excited by unbalances. The stiffness of the stop is usually much higher than that of the flexible bearing.

The rotor is rigid and axial symmetric and supported by symmetrical characteristic bearings. The vibration of the system is described by four degrees of freedom as x_1, y_1, x_2, y_2. The dynamic parameters include:

(1) M: mass of the rotor,
(2) J_d: diameter moment inertia around the mass center,

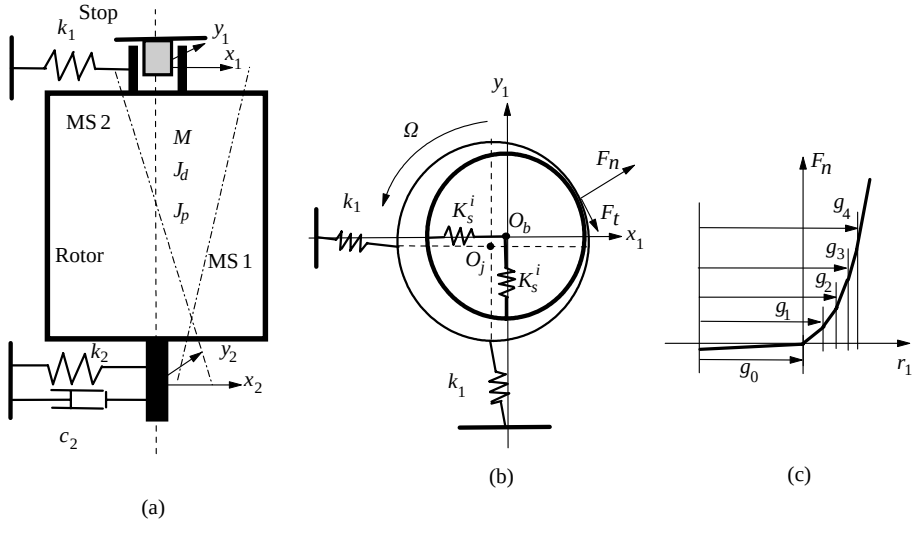

Figure 1. Dynamic model of the rotor-bearing-stop system.

(3) J_p: polar moment inertia around the rotation axis,
(4) k_1: radial stiffness of the top magnetic bearing,
(5) k_2: stiffness of the bottom support,
(6) c_2: damping of the bottom support,
(7) l: height of the rotor,
(8) Ω: rotating speed of the rotor.

The lateral natural vibration equations of the rotor-bearing system are written as

$$\begin{aligned}
&M_{11}\ddot{x}_1 + M_{12}\ddot{x}_2 + H_{11}\dot{y}_1 - H_{11}\dot{y}_2 + k_1 x_1 = 0,\\
&M_{11}\ddot{y}_1 + M_{12}\ddot{y}_2 - H_{11}\dot{x}_1 + H_{11}\dot{x}_2 + k_2 y_2 = 0,\\
&M_{12}\ddot{x}_1 + M_{11}\ddot{x}_2 - H_{11}\dot{y}_1 + H_{11}\dot{y}_2 + k_2 x_2 + c_2\dot{x}_2 = 0,\\
&M_{12}\ddot{y}_1 + M_{11}\ddot{y}_2 + H_{11}\dot{x}_1 - H_{11}\dot{x}_2 + k_2 y_2 + c_2\dot{y}_2 = 0
\end{aligned} \tag{1}$$

in which, $M_{11} = 0{\cdot}25M + J_d/l^2$, $M_{12} = 0{\cdot}25M - J_d/l^2$, $H_{11} = J_p\Omega/l^2$.

Extracting the characteristic roots of equation (1) carries out the natural mode frequencies that alter with increasing rotating speed. The results are illustrated in the Campell diagram (see Figure 2). Because of gyroscope effects, both the first and the second natural modes (with cylindrical mode shape MS1 and conical mode shape MS2 illustrated by Figure 1) split into backward and forward whirl modes at low frequency when the rotor speeds up. The rotor rotates in the counter-clockwise direction set as forward. The rotor-bearing system has two critical speeds at about 300 and 480 r.p.m., respectively, and it runs super-critically at the speed of 3000 r.p.m. Running at 3000 r.p.m., the rotor-bearing system has the first backward whirl mode at the frequency of 4·37 Hz, with the smallest modal damping among the four natural whirl modes.

In the analysis, the rotor/stop rubbing is induced mainly by a certain harmonic excitation under low-frequency because the rotor-bearing system is sensitive to low-frequency

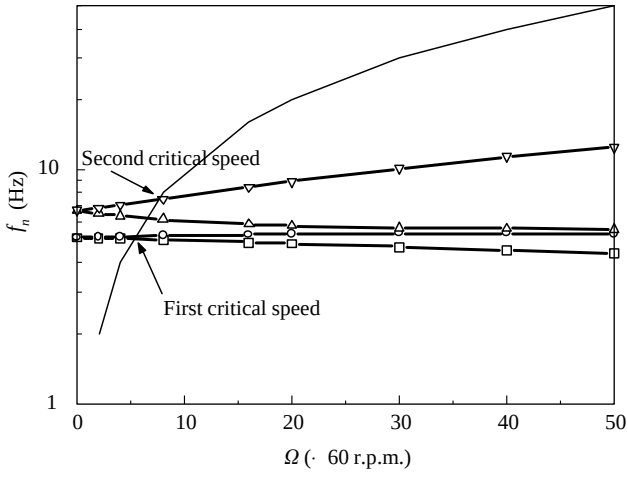

Figure 2. Natural whirl frequencies of the rotor-bearing system. —□—, First backward; —○—, First forward; —△—, Second backward; —▽—, Second forward; $\Omega = f_n$.

disturbances on account of its low-frequency mode with small damping. Moreover, the harmonic excitation is easy to realize in the verification experiments. Including the low-frequency harmonic excitation and the synchronous unbalance excitation, the double-frequency excitation is different from the single synchronous unbalance excitation described in the mentioned references.

At the hollow cylindrical rotor top, it is possible to design two types of stops that are termed as outer and inner type stops. The inner type stop is set to contact with the inner face of the shaft as shown in Figure 1. The impact and friction forces are applied to the rotor by the stop. The friction force will generate forward whirl and tends to suppress the excited backward whirl. On the contrary, the outer type stop is set to rub with the outer face of the journal of the rotor. The friction force generates backward whirl and tends to suppress the excited forward whirl. The tangential friction force from the two types of stops always generates a damping torque to brake the rotation of the rotor.

The forces that come from the bearing and the stop at the top support are written as follows:

$$\begin{aligned} f_k^x &= -k_1 x_1 - F_n \frac{x_1}{r_1} \pm \mu F_n \frac{y_1}{r_1}, \\ & \qquad\qquad \text{while } r_1 < g_0, \quad F_n = 0. \\ f_k^y &= -k_1 y_1 - F_n \frac{y_1}{r_1} \mp \mu F_n \frac{x_1}{r_1}, \end{aligned} \tag{2}$$

In the equation, $r_1 = \sqrt{x_1^2 + y_1^2}$, μ is the friction factor of the stop to the rotor. For the outer type stop, the sign before the friction coefficient is " + ". If the stop is set in the hollow shaft, the sign is " − ". The transient contact force F_n is determined by the rigidity of the stop. Five linear springs with progressively increased stiffness are used to describe the hard spring characteristics of the stop in Figure 1(c).

$$F_n = K_s^{i+1}(r_1 - g_i) + \sum_{j=1}^{i} K_s^j (g_j - g_{j-1}) \quad \text{while } g_i < r_1 < g_{i+1}, \tag{3}$$

if $r_1 < g_i$, then the stiffness coefficients $K_s^{i+1}, K_s^{i+2}, \ldots, K_s^5 = 0$.

$$K_s^1 = f_1 k_1, \quad f_1 \gg f_i,$$

$$K_s^i = f_i K_s^1, \quad i = 2, 3, 4, 5, \tag{4}$$

f_1 is the stop/bearing stiffness ratio, and f_i are the nonlinear spring coefficients. The torque equation of the rotor during rotor/stop rubbing is

$$\frac{\mathrm{d}\Omega}{\mathrm{d}t} J_p = T_m - T_d - \mu F_n R, \tag{5}$$

where T_m is the driven torque of the motor. T_d is the damping torque of the bearing and air friction. R is the radius of the inner face of the rotor top. If rubbing does not occur, then F_n is 0 in equation (5), one can get

$$T_m - T_d = \frac{\mathrm{d}\Omega^*}{\mathrm{d}t} J_p, \tag{6}$$

Therefore, the term of "$T_m - T_d$" is the function of the rotational accelerating speed of the rotor, and it may be measured in the rotor speeding up experiment without rubbing. The lateral forced vibration equations of the rotor-bearing system are written as follows:

$$\begin{aligned}
&M_{11}\ddot{x}_1 + M_{12}\ddot{x}_2 + H_{11}\dot{y}_1 - H_{11}\dot{y}_2 - f_k^x = F_{1x}(t),\\
&M_{11}\ddot{y}_1 + M_{12}\ddot{y}_2 - H_{11}\dot{x}_1 + H_{11}\dot{x}_2 - f_k^y = F_{1y}(t),\\
&M_{12}\ddot{x}_1 + M_{11}\ddot{x}_2 - H_{11}\dot{y}_1 + H_{11}\dot{y}_2 + k_2 x_2 + c_2\dot{x}_2 = F_{2x}(t),\\
&M_{12}\ddot{y}_1 + M_{11}\ddot{y}_2 + H_{11}\dot{x}_1 - H_{11}\dot{x}_2 + k_2 y_2 + c_2\dot{y}_2 = F_{2y}(t).
\end{aligned} \tag{7}$$

The forced excitation terms at the right of the equations are:

$$\begin{aligned}
F_{1x}(t) &= u_1\Omega^2\cos(\Omega t + \alpha) + F\cos(2\pi f_e t),\\
F_{1y}(t) &= u_1\Omega^2\sin(\Omega t + \alpha),\\
F_{2x}(t) &= u_2\Omega^2\cos(\Omega t + \beta),\\
F_{2y}(t) &= u_2\Omega^2\sin(\Omega t + \beta).
\end{aligned} \tag{8}$$

In equation (8), u_1 is the mass unbalance of the rotor top, and α is the phase angle of u_1, u_2 is the mass unbalance of the rotor bottom, and β is the phase angle of u_2. F is the external excitation amplitude, and f_e is the external excitation frequency. To erase the effects of the transient response, the low-frequency excitation is taken into consideration after integrating for 58 s in the calculation. The low-frequency excitation is cut if the rotating speed slows down less than 2400 r.p.m. in severe rubbing. Therefore, the amplitude of the low-frequency excitation is described as follows:

$$F = 0, \quad t < 58\,\mathrm{s}, \qquad F = A(t - 58)/2, \quad 58\,\mathrm{s} \leqslant t \leqslant 60\,\mathrm{s}, \qquad F = A, \quad 80\,\mathrm{s} \geqslant t > 60\,\mathrm{s},$$

$$F = 0, \quad t > 80\,\mathrm{s}, \qquad F = 0, \Omega < 2400\,\mathrm{r.p.m.} \tag{9}$$

The equation systems are solved by the fourth order Runge–Kutta numerical integration method. The motion orbit of the rotor shaft center, the vibration waveforms and the FFT amplitude spectrum are used to describe the dynamic behavior of the system. Although the system has four degrees of freedom, the discussion concentrates on the freedom of x_1 because the external low-frequency force is applied on this freedom and the vibration at the bottom of the system is much smaller than that at the top.

3. SIMULATED PARTIAL AND FULL RUBBING

The numerical simulation on the forced response shows that the external force with a frequency of 4·48 Hz obtains the largest circular backward whirl on applying the force to the rotor at a constant amplitude. Being very near to the first natural backward whirl frequency (4·37 Hz), the excitation frequency of 4·48 Hz is used in the following excitation simulation. The gap between the rotor and the stop is 0·5 mm, much larger than the amplitude (25 μm) of the synchronic unbalance response. The partial rotor/stop rubbing will happen when the excitation amplitude exceeds 0·018 N. As shown in Table 1, five numerical simulation examples are discussed in the following.

Figure 3(a) is the vibration waveform of the rotor excited by the excitation force of 0·013 N, and the orbit of the rotor center is shown in Figure 4(a) and 4(b). The vibration amplitude is not large enough to exceed the gap between the rotor and the stop. Spectrum analysis indicates that the vibration without rubbing is the double-frequency whirl composed of the low-frequency (4·5 Hz) whirl with large amplitude and the synchronic

TABLE 1

Five numerical simulation examples

Example	1	2	3	4	5
A (N)	0·013	0·026	0·15	0·36	0·39
r_1^{max} (mm)	0·28	0·5	0·51	0·52	1·65
Rubbing	None	Light partial	Hard partial	Hard partial	Full

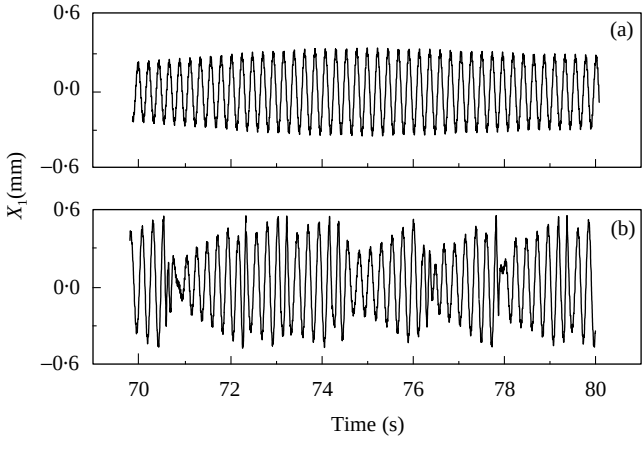

Figure 3. Vibration waveform. (a) $A = 0{\cdot}13$ N; (b) $A = 0{\cdot}026$ N.

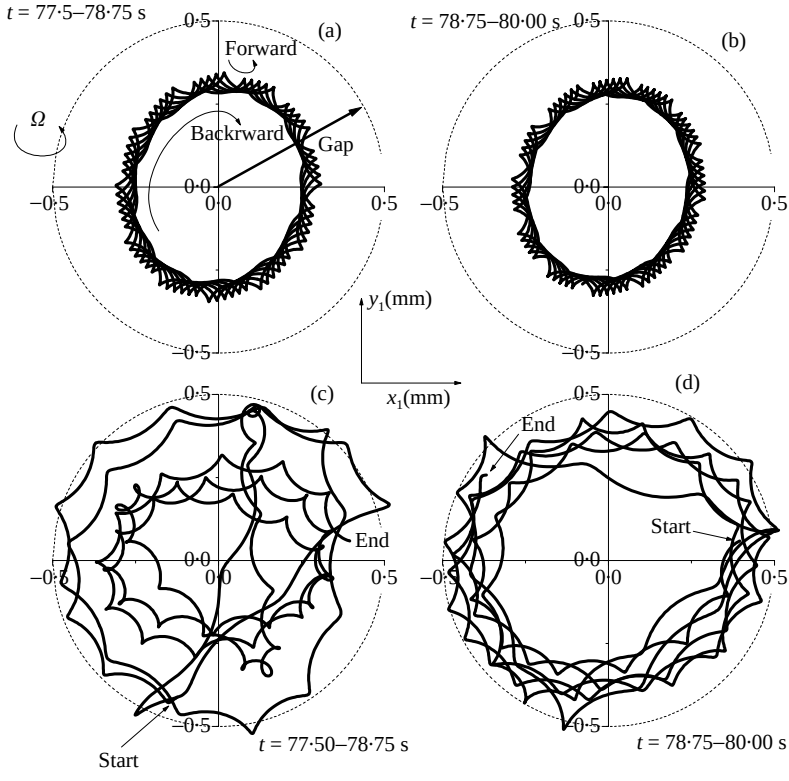

Figure 4. Motion orbits of the rotor center.

(50 Hz) whirl with small amplitude. As shown in Figure 4(a) and 4(b), the outline of the orbit displays the low-frequency asynchronous circular whirl due to the external excitation, and the local small winding displays the synchronous forward whirl caused by the unbalance. Since the outline of the rotor center moves clockwise, the large whirl in low frequency is backward.

In the second example, the excitation amplitude equals to 0·026 N, the rotor contacts the stop several times when the vibration exceeds the rotor/stop gap. As shown in Figure 3(b), the increasing forced vibration of the rotor is restricted by the stop when the partial rubbing occurs; then the vibration decreases because of the impact and friction between the rotor and the stop. The suppressed vibration will grow until the next rubbing because the excitation is still acting. The turbulent motion orbits of the rotor center with rubbing are shown in Figure 4(c) and 4(d).

In the third and fourth numerical simulation examples, the excitation amplitude rises to 0·15 N and 0·36 N. The vibration of the partial rubbing becomes more turbulent, which was shown in Figures 5(a) and 5(b). As shown in Figure 6(a), for the light partial rubbing example, the rotating speed only fluctuates slightly around 3000 r.p.m., which is the result of the friction damping torque and the driven torque of the motor. For the example of severe partial rubbing case, the rotating speed has a drop of less than 1% in 10 s, which is shown in Figure 6(b). The multiple impact and friction in the severe partial rubbing has a significant effect on the rotating of the rotor. During the partial rubbing, the rotor contacts the stop occasionally and transiently, the rotor's rotating speed remains almost at 3000 r.p.m. (light partial rubbing) or has a drop of less than 1% (severe partial rubbing) and the stop restricts the vibration amplitude of the rotor effectively.

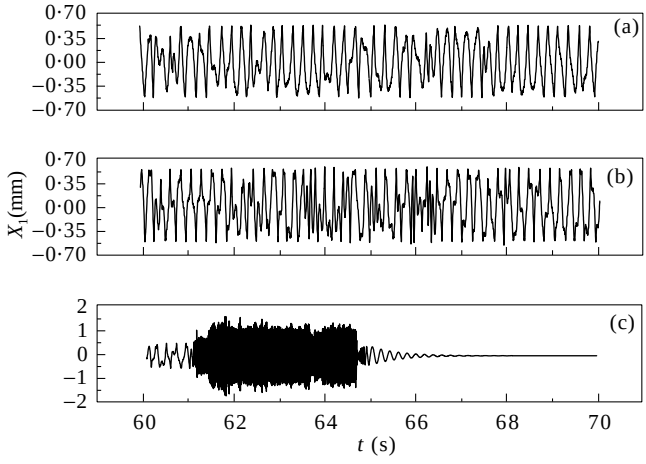

Figure 5. Vibration waveform. (a) $A = 0{\cdot}15$ N; (b) $A = 0{\cdot}36$ N; (c) $A = 0{\cdot}39$ N.

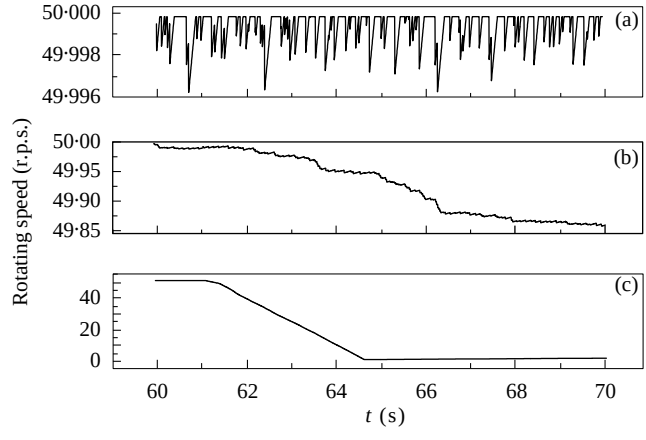

Figure 6. Changes of the rotating speed under different excitations. (a) ○; (b) △; (c) ⊙.

The rubbing vibration of the rotor changes greatly when the excitation amplitude arrives at 0·39 N (see Figure 5(c)). The turbulent vibrating rotor falls into whipping at a much higher frequency with amplitudes larger than the rotor/stop gap. The rotor rolls on the stop without separation. The continuous full rubbing slows down the rotating speed of the rotor very quickly. As shown in Figure 6(c), the rotating speed drops from 50 r.p.s. down to nearly 0 r.p.s. in 3 s. At the same time, the friction force sustains the high-frequency whip for about 3 s. The rotating kinetic energy of the rotor is dissipated quickly through friction. From the zoomed vibration and rotating speed diagram in Figure 7, one can see that the rotor separates from the stop and ceases from rotating at the 64.64th second. There exists a transient state after the rotor separates from the stop, and the rotating speed rises linearly at the driven torque after the 64·64th s. The vibrations die out almost after around the 66th second because there exists no external excitation and the unbalance excitation is very small at the very low rotating speed.

Figures 8 and 9 show the orbits of the rotor center that whirl with partial rubbing and then expand to whip with full rubbing, during the sampling time from the 60th to the 65th s.

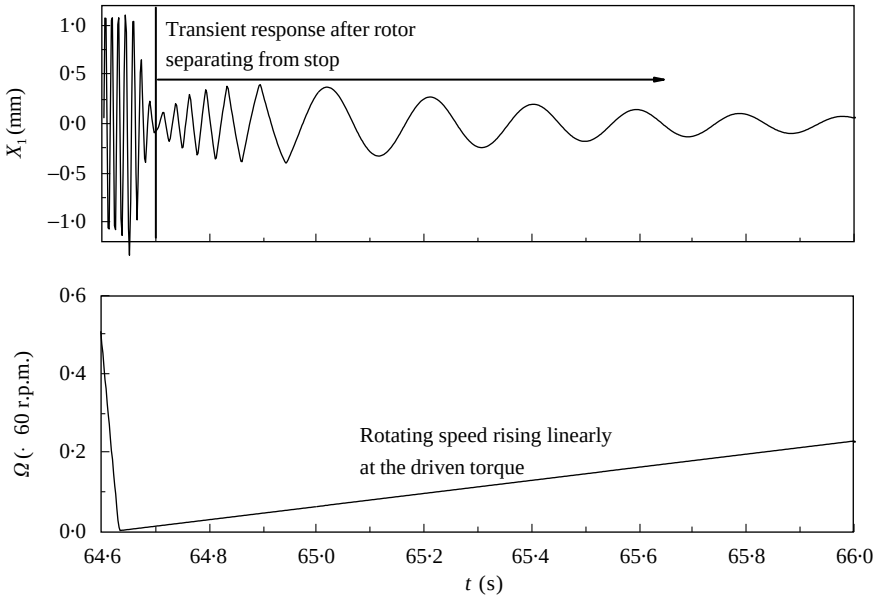

Figure 7. Vibration and rotating speed after full rubbing.

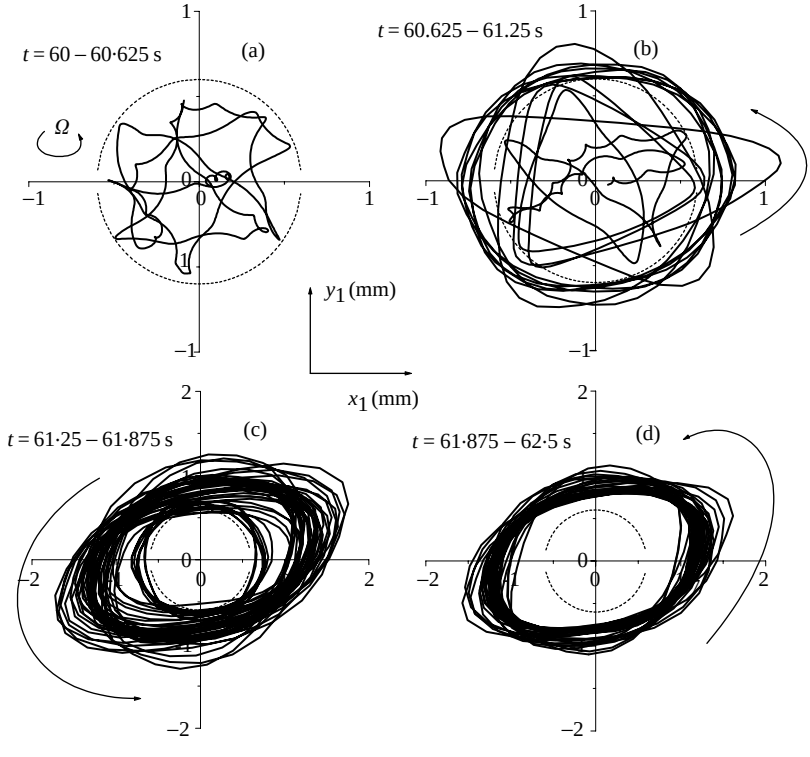

Figure 8. Motion orbits of the rotor center in full rubbing.

The results in Figure 10 of FFT analysis on the vibration indicate that the low-frequency whirl turns into high-frequency whip when the partial rubbing turns into full rubbing. During the sampling time from the 60th to the 60·625th s, the dominant frequency of the

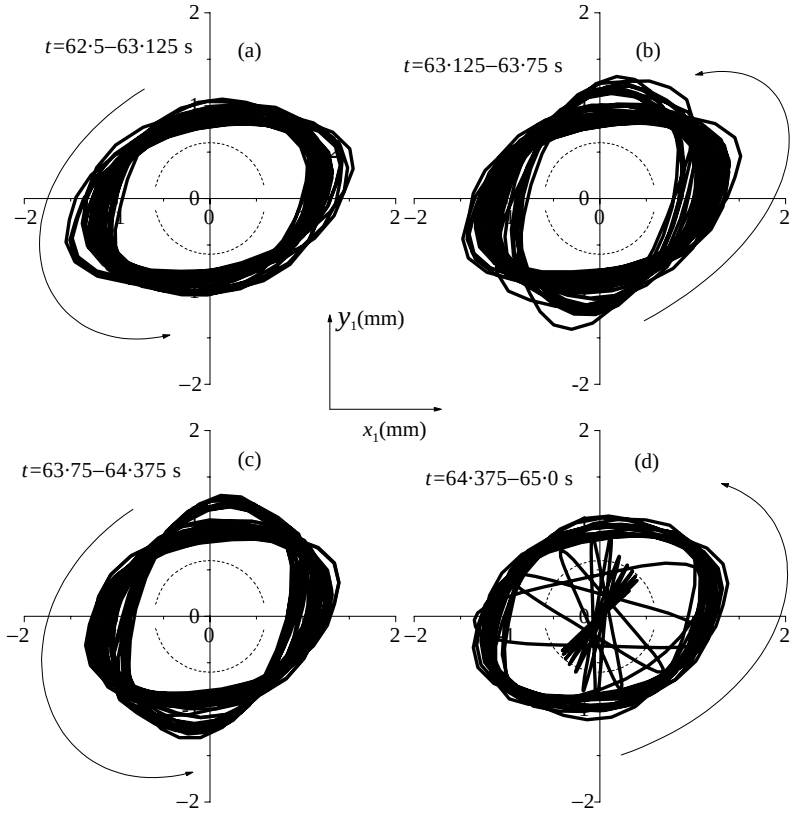

Figure 9. Motion orbits of the rotor center in full rubbing.

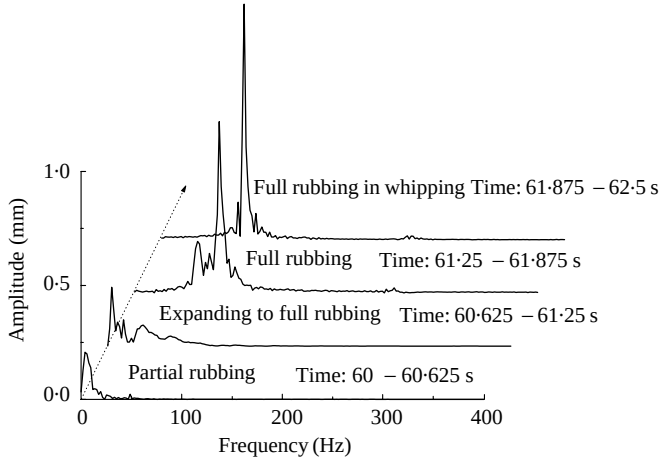

Figure 10. FFT spectrum analysis results.

vibration FFT analysis is 4·5 Hz. The occurrance of higher frequency indicates that the full rubbing is generated during the time from the 60·625th to the 61·25th s. After 61·25 s, the disappearance of the frequency of 4·5 Hz and the appearance of the higher frequency with

a large spectrum value indicate that the rotor contacts the stop without separation. Then the rotor whips violently with a high frequency of 80 Hz that seems to be the natural mode frequency of the new system in which the inertia part is the rotor and the stop is the elastic element.

During the full rubbing, the center of the rotor whirls forward or counter-clockwise, the whip amplitude exceeds the rotor/stop gap abruptly, and the frequency of the whip is much higher than that of the excitation and the unbalance force. The rotor rotation is also broken quickly by the stop in the full rubbing.

4. SELECTION OF THE STOP STIFFNESS

The full rotor/stop rubbing will be induced only after the excitation is great enough. It is desirable to enlarge the scope of the excitation without causing full rubbing. Being a fundamental parameter, the stop stiffness has a significant effect on the initiation of the full rubbing. The minimum excitation causing the full rubbing at different stop stiffnesses is illustrated in Table 2. From the data in the table, one can see that the higher the stop stiffness, the smaller is the excitation. Therefore, the stop stiffness should be selected as lower to ensure the partial rubbing excited by the large excitation.

However, the stop stiffness should not be too low because the stop is set to limit the vibration amplitude. If it is too low, the stop cannot restrict the vibration amplitude effectively, which is indicated by Table 3. For example, if the over-limit ratio O_s is restricted less than 10%, then the stiffness ratio should be more than 100. O_s is defined as

$$O_s = (r_l^{max} - g_0)/g_0 \times 100\%. \tag{10}$$

To describe the contact duration in the rubbing experiment, the contact ratio is defined as

$$r_c = \frac{\sum_{i=1}^{n} T_c^i}{T_e} \times 100\%. \tag{11}$$

T_c^i is the rotor/stop contact duration, T_e is the acting time of low-frequency external excitation. As shown in Table 4, the contact ratio becomes smaller when the stop stiffness increases. Since the rubbing may hurt the rotor and the stop; therefore, the contact ratio should be as low as possible. Increasing the stop stiffness reduces the contact ratio. The initiation of full rubbing, the over-limit ratio and the contact ratio together suggest that the

TABLE 2

Initiation of full rubbing at different stop/bearing stiffness ratios

f_1	100	200	400	600	800
A (N)	0·94	0·53	0·39	0·26	0·20

TABLE 3

Over-limit ratio at different stop/bearing stiffness ratios

f_1	5	10	20	50	100	200	400
O_s	36	22	16	12	8	6	5

TABLE 4

Contact ratio at different stop/bearing stiffness ratios

f_1	5	10	20	50	100	200	400	600	800
r_c	51·6	30·0	17·1	10·4	7·66	5·33	3·58	3·15	2·45

suitable stop/bearing stiffness ratio should be from 100 to 400 for the rotor under consideration. For different rotor-bearing systems, the suitable stop/bearing stiffness ratio may be different. However, it is valuable and practical to consider the criteria of the initiation of the full rubbing, the over-limit ratio and the contact ratio.

5. EXPERIMENTAL VERIFICATION

The rotor/stop rubbing experiments are done to verify the feasibility and the limitation of using stops to control the large vibration of rotors. The experimental set-up is mainly composed of the following four parts: the rotor and motor, the exciter, the test instruments and the data collector and analyzer.

The motor's power frequency is 50 Hz. The rotor speeds up to 3000 r.p.m. in about 5 min. The exciter is an electromagnetic actor. It is set close to the rotor top support to perturb the magnetic field of the permanent magnetic bearing. The sinusoid signal from the signal generator is amplified and then drives the exciter to generate a synchronous harmonic excitation. The frequency of the excitation and the amplitude vary to satisfy the experiments. To measure the excitation amplitude, a DC volt is applied to the electromagnetic actor, which leads to the rotor drifting off the central axis of the bearings. Then a compensation elastic force pushes the rotor to its original center position. On measuring the elastic force one obtains the relation between the DC volt and the force. The excitation amplitude varies from 0 to 0·48 N according to the amplitude of the volt signal. The XY displacement probes test the radial displacement of the rotor top and bottom. The photoelectric sensor obtains the rotating speed of the rotor. The sound sensor picks up the impact sound as rotor/stop rub takes place. The test data are observed by the oscilloscope, analyzed by the dynamic signal analyzer and collected by a macro-computer data collecting system.

The test rotor is the origin of the above theoretical model. The experimental rubbing conditions are basically designed to suit the numerical simulation parameters. The rotor/stop gap is 0·5 mm. The stop/bearing stiffness ratio is 400.

The following steps are performed in the rubbing experiments. Firstly, the rotor is brought to run at the speed of 3000 r.p.m. Then the proper excitation frequency of 4·4 Hz is found to obtain the largest response of the rotor top through sweeping sine excitation tests. At that frequency, the excitation force is increased until the peak amplitude of rotor whirl becomes large enough to exceed the gap of rotor/stop. The transducers and data test systems measure and record the dynamic behavior of the rubbing rotor, including the vibration time history, the frequency spectrum of vibration and the orbits of the rotor center.

Similar to the numerical results, the rotor contacts the stop when the excitation arrives at 0·02 N. The rotor/stop rubbing retains partial characteristics even if the excitation increases to 0·29 N. As illustrated by Figure 11, the stop restricts the amplitude of the vibration very effectively. The linear forced response is in proportion to the external excitation without the stop's restriction. But the vibration amplitude remains at almost the value of the gap when

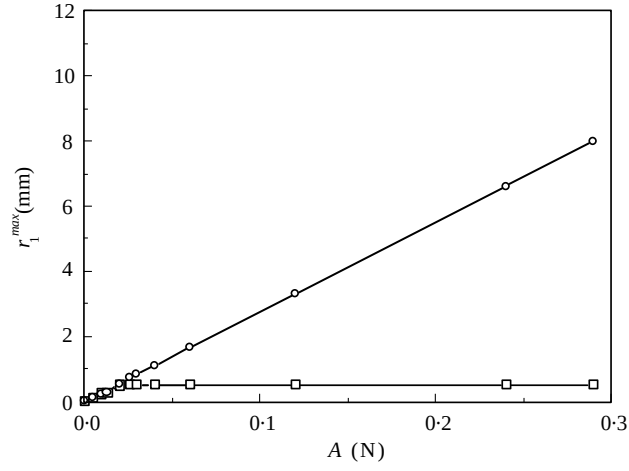

Figure 11. The limit function of the stop. —□—, with partial rubbing (test results); —○—, without rubbing (theoretical prediction).

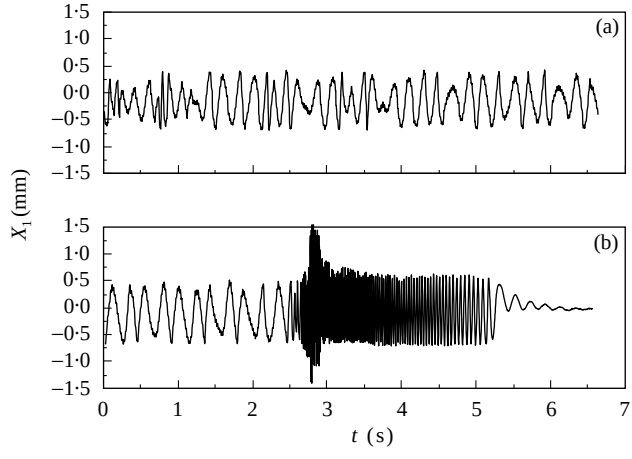

Figure 12. Vibration waveform of partial rubbing and full rubbing. (a) $A = 0{\cdot}29$ N; (b) $A = 0{\cdot}33$ N.

the stop acts. The rotor contacts the stop occasionally. The impact and the friction between the rotor and the stop suppress the vibration of the rotor. The constant output of the rotation speed transducer indicates that the friction torque has not exceeded the motor-driven torque. The vibration waveform in Figure 12(a) shows the turbulent character predicted by the numerical simulation.

Figure 12(b) depicts the vibration of the rotor excited by the excitation of 0·33 N that is smaller than the full rubbing excitation (0·39 N) in the numerical simulation. The low-frequency whirl with partial rubbing turns into full rubbing at high-frequency whip. The frequency of the whip grows as high as 350 Hz in an instant and then slows down quickly. In contrast, the calculated whip frequency remains almost constant at a value of 80 Hz. The amplitude of the whip is larger than the rotor/stop gap limit. Figure 13 shows the orbits of the rotor in full rubbing. At the same time, the test rotating speed of the rotor drops from 3000 r.p.m. down to nearly 0 r.p.m. in 3 s because of the continuous rotor/stop friction, which is shown in Figure 14. The predicted results in terms of the turbulent whirl turning

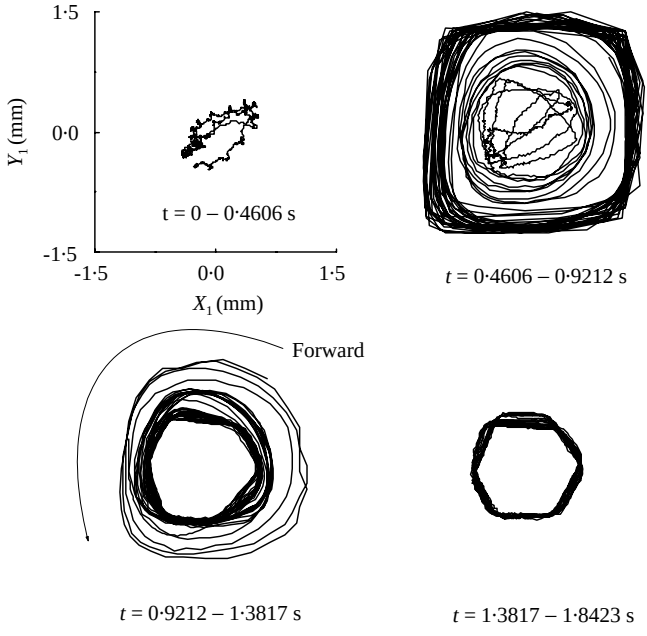

Figure 13. Motion orbits of the rotor center in full rubbing.

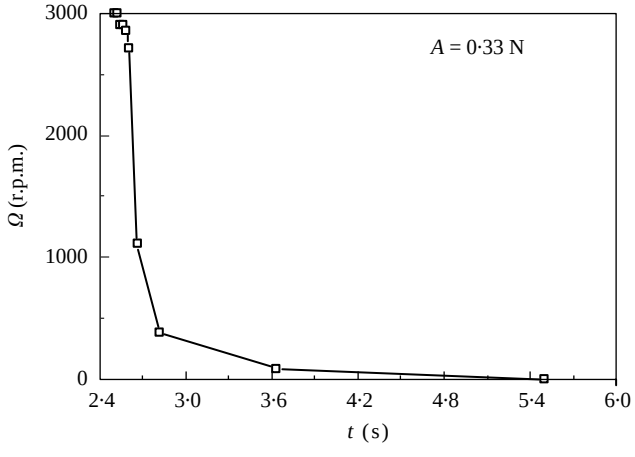

Figure 14. Test rotating speed in full rubbing.

into forward whipping after full rubbing initiation and the diminishing of the rotating speed agreed with the test results.

After the rubbing experiments, a lot of metal powder was found on the inner face of the rotor top, which means that the continuous serious friction does harm to the stop and the rotor face. The stop loses its restricting function in full rubbing; the possible rubs at other positions may cause serious damage to the rotor. Therefore, full rubbing must be avoided when using the stop to control the vibration of the rotor.

To verify the effect of the stop stiffness on the initiation of the full rubbing, three comparison tests are carried out. The experimental results in Table 5 confirm that the more rigid the stop is, the smaller the excitation causing the full rubbing.

TABLE 5

Maximum excitation and rubbing types in experiments

Gap (mm)	A_{max}/Types	A_{max}/Types	A_{max}/Types
0·7	0·48/Partial	0·40/Full	0·26/Full
0·5	0·48/Partial	0·33/Full	0·18/Full
0·4	0·40/Full	0·13/Full	0·08/Full
Stiffness ratio	200	400	600

6. CONCLUSIONS

(1) The multiple segments linear spring model is used to investigate the dynamic behavior of the rotor under rotor/stop rubbing. The simulation and experiments on the rotor/stop rubbing demonstrate that the inner-type stop suppresses the low-frequency backward whirl successfully. It is practical to use stops to limit the violent vibration of rotors supported by low-stiffness bearings.

(2) When the amplitude of the force exceeds a certain value, full rubbing occurs with continuous serious friction. In the full rubbing, the center of the whipping rotor moves counter-clockwise, the whip amplitude exceeds the rotor/stop gap abruptly. Moreover, the whip frequency is much higher than that of the excitation and the unbalance force. The rotor rotation is broken quickly by the stop. The predicted dynamic behavior is verified well by the full rubbing experiments. Full rubbing should be prevented since it does great harm to the stop and the rotor.

(3) The discussion on the criteria of the initiation of full rubbing, the over-limit ratio and the contact-ratio suggests that the suitable stop/bearing stiffness ratio should be from 100 to 400 for the rotor under consideration. It is valuable and practical to use the criteria to select the stop stiffness.

REFERENCES

1. D. W. CHILDS 1979 *American Society of Mechanical Engineers Journal of Mechanical Design* **10**, 640–644. Rub induced parametric excitation in rotors.
2. O. MATSUSHITA, M. TAKAGI and K. KIKUCHI 1984 *Bulletin of JSME* **27**, 278–288. Analysis of rotor vibration excited by seismic wave.
3. F. K. CHOY and J. PADOVAN 1987 *Journal of Sound and Vibration* **113**, 529–544. Non-linear transient analysis of rotor-casing rub events.
4. P. GOLDMAN and A. MUSZYNSKA 1994 *American Society of Mechanical Engineers Journal of Vibration and Acoustics* **116**, 692–701. Chaotic behavior of rotor/stator systems with rubs.
5. P. GOLDMAN and A. MUSZYNSKA 1994 *American Society of Mechanical Engineers Journal of Vibration and Acoustics* **116**, 541–547. Dynamics effects in mechanical structures with gaps and impacting: order and chaos.
6. F. ERICH 1988 *American Society of Mechanical Engineers Journal of Vibration, Acoustics, Stress, and Reliability in Design* **110**, 9–16. High order subharmonic response of high speed rotors in bearing clearance.
7. F. ERICH 1991 *American Society of Mechanical Engineers Journal of Vibration and Acoustics* **113**, 50–57. Some observations of chaotic vibration phenomena in high speed rotordynamics.
8. F. CHU and Z. ZHANG 1998 *Journal of Sound and Vibration* **210**, 1–18. Bifurcation and chaos in a rub-impact jeffcott rotor system.
9. X. J. DAI, X. Z. ZHANG and Z. X. JIN 1998 *Journal of Tsinghua University Science and Technology* **38**, 104–106. Dynamic behavior of a precession rotor having impact and rub with stop.
10. S. YANABE, S. KANEKO, Y. KANEMITSU, N. TOMI and K. SUGIYAMA 1998 *American Society of Mechanical Engineers Journal of Vibration and Acoustics* **120**, 544–550. Rotor vibration due to collision with annular guard during passage through critical speed.

11. T. ISHHII and R. G. KIRK 1996 *American Society of Mechanical Engineers Journal of Vibration and Acoustics* **118**, 154–163. Transient response technique applied to active magnetic bearing machinery during rotor drop.
12. G. T. FLOWERS, H. XIE and S. C. SINHA 1995 *NASA Technical Report N*95-32691. Dynamic behavior of a magnetic bearing supported jet engine with auxiliary bearings.
13. X. WANG and S. NOAH 1998 *American Society of Mechanical Engineers Journal of Vibration and Acoustics* **120**, 596–606. Nonlinear dynamics of a magnetically supported rotor on safety auxiliary bearings.
14. A. MUSZYNSKA, W. D. FRANKLIN and R. D. HAYASHIDA 1992 *NASA Technical Report N*92-14367. Rotor-to-stator partial rubbing and its effects on rotor dynamic response.
15. A. M. FREE and G. T. FLOWERS 1995 *NASA Technical Report N*95-32692. Dynamic modeling and response characteristics of a magnetic bearing rotor system with auxiliary bearings.